PNAS RESEARCH ARTICLE | NEUROSCIENCE

Basal forebrain cholinergic activity is necessary for upward firing rate homeostasis in the rodent visual cortex

Juliet Bottorff[a], Sydney Padgett[a], and Gina G. Turrigiano[a,1]

Contributed by Gina G. Turrigiano; received October 16, 2023; accepted November 22, 2023; reviewed by Daniel E. Feldman and Tara Keck

Bidirectional homeostatic plasticity allows neurons and circuits to maintain stable firing in the face of developmental or learning-induced perturbations. In the primary visual cortex (V1), upward firing rate homeostasis (FRH) only occurs during active wake (AW) and downward during sleep, but how this behavioral state-dependent gating is accomplished is unknown. Here, we focus on how AW enables upward FRH in V1 of juvenile Long Evans rats. A major difference between quiet wake (QW), when upward FRH is absent, and AW, when it is present, is increased cholinergic (ACh) tone, and the main cholinergic projections to V1 arise from the horizontal diagonal band of the basal forebrain (HDB ACh). We therefore chemogenetically inhibited HDB ACh neurons while inducing upward homeostatic compensation using direct activity-suppression in V1. We found that synaptic scaling up and intrinsic homeostatic plasticity, two important cellular mediators of upward FRH, were both impaired when HDB ACh neurons were inhibited. Most strikingly, HDB ACh inhibition flipped the sign of intrinsic plasticity so that it became anti-homeostatic, and this effect was phenocopied by knockdown of the M1 ACh receptor in V1, indicating that this modulation of intrinsic plasticity is the result of direct actions of ACh within V1. Finally, we found that upward FRH induced by visual deprivation was completely prevented by HDB ACh inhibition. Together, our results show that HDB ACh modulation is a key enabler of upward homeostatic plasticity and FRH, and more broadly suggest that neuromodulatory inputs can segregate upward and downward homeostatic plasticity into distinct behavioral states.

cholinergic modulation | homeostatic plasticity | synaptic scaling | intrinsic plasticity | sleep

Neocortical networks have the remarkable capacity to change in response to experience, while simultaneously maintaining stable function over the lifetime of an organism. This stability is accomplished through a set of homeostatic negative feedback mechanisms that can compensate for perturbations driven by development or learning-induced plasticity (1–3) and act to stabilize key features of network function such as firing rates, correlation structure, and information-carrying capacity (4–6). In the primary visual cortex (V1), mean firing rates are one important target of homeostatic regulation: Closing one eye (monocular deprivation, MD) initially suppresses firing, but firing then slowly (over 2 to 3 d) regulates back to baseline even though the eye remains closed (4, 7). This process is bidirectional, as re-opening the eye after compensation has occurred initially drives an overshoot of firing, which is again followed by a slow return to baseline (8). A striking feature of this firing rate homeostasis (FRH) is that upward and downward regulation are segregated into distinct behavioral states: While downward FRH occurs exclusively during sleep (8), upward FRH is confined to periods of active wake (AW) (4). This suggests that the cellular homeostatic plasticity mechanisms that underlie FRH are gated by feature(s) that are specific to sleep or wake states, but what these features might be is unknown. Here, we test the hypothesis that the induction of synaptic and intrinsic mechanisms underlying upward FRH is enabled by wake-active cholinergic modulation within V1.

The cellular plasticity mechanisms that contribute to FRH in rodent V1 during the classic visual system critical period have been explored in some detail. In particular, upward FRH is correlated with the induction of both synaptic scaling up and intrinsic homeostatic plasticity (7, 9, 10); by increasing excitatory synaptic drive and the ability of synaptic inputs to elicit spikes, these changes are in the right direction to restore firing in these neurons. Further, these two forms of homeostatic plasticity are jointly induced in L2/3 pyramidal neurons when their firing is directly suppressed using chemogenetics (11). Finally, both synaptic scaling and intrinsic homeostatic plasticity are absent in a genetic manipulation (loss of the multidomain scaffold protein Shank3) that prevents upward FRH (11, 12), suggesting that these two forms of homeostatic plasticity are essential for the expression of upward FRH. How the induction of synaptic scaling and intrinsic

Significance

Sleep and wake states influence learning and behavior by modulating many forms of experience-dependent plasticity, including homeostatic mechanisms that stabilize circuit function; how this occurs at the cellular level is poorly understood. Upward homeostasis of neuronal activity during sensory deprivation in visual cortex is confined to active waking states; here, we show that wake-active cholinergic inputs are essential for this homeostatic recovery. Inhibiting these inputs impairs two major cellular forms of upward homeostatic plasticity (synaptic scaling and intrinsic homeostatic plasticity), in part through direct activation of local muscarinic acetylcholine receptors, and prevents activity in visual cortex from undergoing homeostatic recovery. This suggests neuromodulatory inputs during specific vigilance states can orchestrate plasticity within neocortical circuits to promote homeostatic recovery of activity.

Author affiliations: [a]Department of Biology and Neuroscience Program, Brandeis University, Waltham, MA 02453

Author contributions: J.B. and G.G.T. designed research; J.B. and S.P. performed research; J.B., S.P., and G.G.T. analyzed data; and J.B. and G.G.T. wrote the paper.

Reviewers: D.E.F., UC Berkeley; and T.K., University College London.

The authors declare no competing interest.

[1]To whom correspondence may be addressed. Email: turrigiano@brandeis.edu.

This article contains supporting information online at https://www.pnas.org/lookup/suppl/doi:10.1073/pnas.2317987121/-/DCSupplemental.

Published December 26, 2023.

homeostatic plasticity might be enabled by AW and suppressed during other behavioral states is unknown.

Sensory inputs and neural activity patterns are dramatically different during wake and sleep, but the difference between quiet wake (QW), when upward FRH is absent, and AW, when it is robustly induced, is much subtler and largely due to differences in the activity of neuromodulatory systems (13–15). In particular, increased cholinergic modulation is a key signature of AW, and optogenetic stimulation of cholinergic neurons in the basal forebrain can promote fast transitions from non-rapid eye movement sleep (NREM) to AW (15–17). Notably, cholinergic innervation is important for the expression of ocular dominance plasticity in V1 (18), which relies on homeostatic plasticity (3, 19), and cholinergic modulation can enhance visual learning (20, 21). Cholinergic inputs to rodent V1 come almost exclusively from the horizontal diagonal band (HDB) of the basal forebrain (BF), and these HDB cholinergic (HDB ACh) neurons fire at high rates during AW and are almost silent during NREM and QW (22–24). Thus, we hypothesized that activity of V1-projecting HDB ACh neurons is necessary for the induction of AW-gated upward homeostatic plasticity within V1.

To test this hypothesis we used a Chat-Cre Long Evans rat strain to selectively express inhibitory DREADDs in HDB ACh neurons, allowing us to chronically inhibit these neurons during the induction of homeostatic plasticity in V1. We then combined HDB ACh inhibition with direct chemogenetic suppression of activity in V1 to induce homeostatic plasticity (11) and targeted L2/3 pyramidal neurons for ex vivo whole cell recordings. We found that reducing the activity of HDB ACh inputs alone modestly increased excitatory quantal amplitude and prevented synaptic scaling up. More strikingly, HDB ACh inhibition flipped the sign of intrinsic plasticity from a homeostatic increase to an anti-homeostatic decrease. To test whether this effect was due to reduced cholinergic signaling within V1, we knocked down the abundant Gq-coupled M1 ACh receptor in V1 and found that this phenocopied the effects of HDB ACh inhibition on intrinsic plasticity. Finally, we asked whether HDB ACh neuron inhibition prevents upward FRH during prolonged MD. Indeed, initiating HDB ACh inhibition after 2 d of MD (when firing rates had dropped) completely prevented the normal homeostatic recovery of firing rates. Taken together, our data show that HDB ACh activity is critical for the normal expression of two important forms of cellular homeostatic plasticity that cooperate to increase excitability and is required for upward FRH. These data suggest that AW enables upward homeostatic plasticity by enhancing cholinergic modulation within V1.

Results

Long-Lasting Inhibition of V1-Projecting HDB ACh Neurons using DREADDs. We wished to know whether the activity of HDB ACh neurons can modulate the induction of homeostatic plasticity in V1 L2/3 pyramidal neurons. To chronically suppress the activity of HDB ACh neurons, we used a viral vector expressing a Cre-dependent form of the inhibitory DREADD Hm4di (AAV9-hSyn-DIO-hM4D(Gi)-mCherry). After injecting this vector into the HDB of ChAT-Cre rats and waiting 2 wk, we performed immunostaining against ChAT to label HDB ACh neurons and found robust expression of Hm4di-mCherry in ChAT-positive cell bodies (Fig. 1 *A* and *B*, *Left* panels), as well as in their axonal projections to V1 (Fig. 1 *A* and *B*, *Right* panels).

We next confirmed that Hm4di expression was able to effectively inhibit HDB ACh neurons upon administration of the exogenous ligand CNO. At least 1 wk after viral delivery of Hm4di, ChAT-cre rats were given ad libitum access to CNO in their drinking water (11) for either 0, 12, or 48 h prior to killing at Zeitgeber (ZT) 01:00; animals were kept awake for 1 h prior to killing (ZT 00:00–01:00) using gentle handling to ensure some baseline level of HDB ACh neuron activity. We then performed immunostaining on HDB slices and probed for RFP expression (indicating an Hm4di+ cell) and cFos expression (an indicator of neural activity). Both 12 and 48 h of CNO produced a ~50% reduction in the fraction of HDB ACh neurons that were cFos+ (Fig. 1 *C* and *D*), indicating that we can achieve a long-lasting inhibition of their activity. As an additional control, we quantified cFos expression in HDB ACh neurons with no viral DREADD expression (using immunostaining against Chat); these two control groups had very similar levels of baseline cFos expression (no virus, no CNO: 19.27 ± 1.57%; Hm4di, no CNO: 21.53 ± 3.72%), so these two control groups were combined (Fig. 1*D*).

Manipulation of BF ACh neurons can induce significant changes in cortical rhythms. Optogenetic activation decreases delta band and increases theta band power (16, 20, 23), while inhibiting them increases delta band power (20, 25, 26). To determine whether HDB ACh inhibition using Hm4Di affects brain-state activity within V1, we used local field potential (LFP) recordings to quantify the average LFP power in three different frequency bands (Delta, Theta, and Alpha) in the 8 h immediately following subcutaneous CNO injections (3 mg/kg), normalized to time- and circadian-matched periods from the same animals on recording days with no CNO administration. As expected, inhibition of HDB ACh neurons significantly increased delta power, while alpha power was significantly decreased (Fig. 1 *E* and *F*), indicating that HDB ACh inhibition has a measurable impact within V1.

Chronic inhibition of HDB ACh neurons is reported to have small and variable effects on total amount of sleep and wake (26–29). To verify that HDB ACh inhibition did not produce major changes in total sleep and wake we used LFP, electromyography (EMG), and video recordings to quantify the amount of time Hm4di-expressing animals spent in each of four behavioral states (Active Wake, AW; Quiet Wake, QW; Rapid Eye Movement sleep, REM; and Non-REM, NREM, sleep) in the 8 h immediately following CNO administration, normalized to time- and circadian-matched periods with no CNO administration. We found that rats spent comparable amounts of time in AW, QW, and NREM sleep before and after HDB ACh inhibition, but there was a small decrease in time spent in REM sleep (Fig. 1*G* and *SI Appendix*, Table S1). Because rats normally spend little time in REM sleep (~10%; see *SI Appendix*, Table S1), this small reduction in REM corresponds to very little change in total sleep. Taken together, our results show that we can chronically reduce the activity of cholinergic projections to V1 without dramatically influencing total sleep/wake time.

HDB ACh Inhibition Impairs Synaptic Scaling. Having established that we can effectively inhibit HDB ACh activity, we next asked whether this inhibition impairs the induction of homeostatic plasticity within V1. L2/3 pyramidal neurons in V1 express two major forms of homeostatic plasticity during the critical period: synaptic scaling and intrinsic homeostatic plasticity (7, 9, 12, 30, 31), both of which can be directly induced through Hm4Di-mediated inhibition of L2/3 pyramidal neurons for 24 to 48 h (11). We therefore inhibited L2/3 pyramidal neuron activity with or without simultaneous HDB ACh inhibition, then recorded from L2/3 pyramidal neurons to assess their synaptic and intrinsic properties.

To accomplish this, we virally delivered CaMKII-driven inhibitory DREADDs (AAV9-CaMKII-hM4D(Gi)-mCherry)

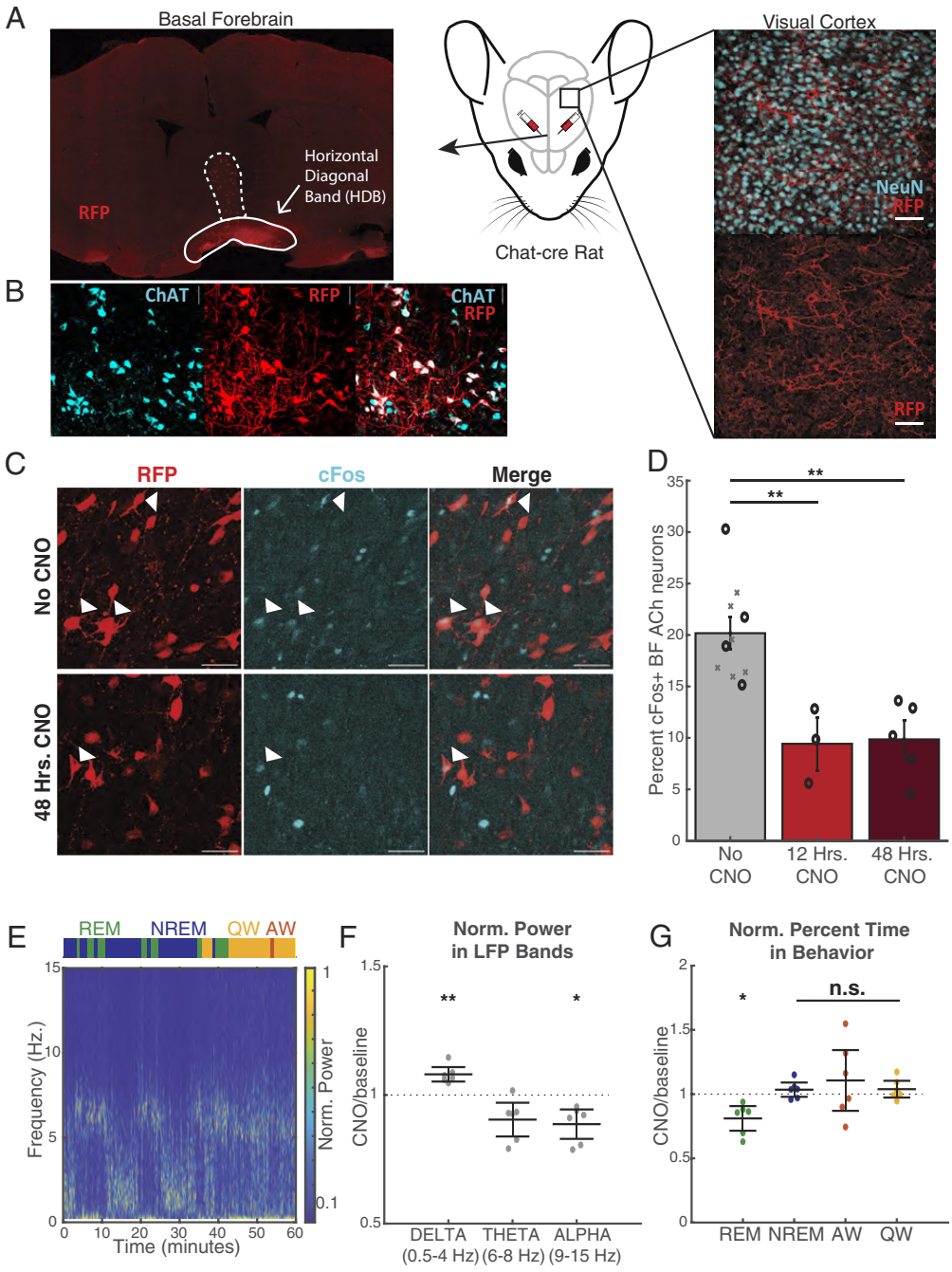

Fig. 1. Long-lasting inhibition of V1-projecting HDB ACh neurons using DREADDs. (*A*) Schematic of viral injection of AAV-hsyn-DIO-hM4D(Gi)-mCherry into HDB of ChAT-cre rats (*Center*; rat head adapted from Scidraw) and example images of the resulting mCherry+ cell bodies in the basal forebrain (*Left*) and their mCherry+ projections in the visual cortex (*Right*). RFP labels the mCherry tag. *Left* image: Basal forebrain; solid line indicates basal forebrain region of interest, the horizontal diagonal band (HDB); dashed line indicates vertical diagonal band, another region of the basal forebrain; 10x magnification; red = RFP. *Right* image: Visual cortex; scale bar = 50 μm; cyan = NeuN; red = RFP. (*B*) mCherry expression from virus injections is restricted to ChAT+ neurons in ChAT-cre rats. Scale bar = 50 μm; cyan = ChAT; red = RFP. (*C*) Example images of cFos and mCherry expression after virus injections into the HDB of ChAT-cre rats. The top row is from an animal without any exposure to CNO; the bottom row is from an animal that received CNO in its drinking water for 48 h prior to killing. Scale bar = 50 μm; cyan = cFos; red = RFP. (*D*) Quantification of cFos expression in HDB ACh neurons, showing ~50% reduction in cFos expression after either 12 or 48 h of CNO exposure. All animals in the 12-h CNO (N = 5) and 48-h CNO (N = 5) groups had Hm4di-mCherry in BF ACh neurons, and quantification was evaluated as the percent of RFP+ HDB neurons that were cFos+. The No CNO group includes four animals with Hm4di-mCherry in HDB ACh neurons (black circles) and six animals without virus injection (gray X's). The Hm4di-mCherry animals were quantified as above, and the no virus injection animals were quantified as the percent of ChAT+ HDB neurons that were cFos+. We note that there was no difference in these two No CNO groups, indicating no effect of Hm4di-mCherry on basal HDB ACh neuron activity, so we combined the two groups here. P = 0.00018, 1-way ANOVA with Tukey's post hoc. No CNO vs. 12 h. CNO: P = 0.0011; No CNO vs. 48 h. CNO: P = 0.0009. (*E*) Example LFP spectrogram and behavior from 1 h of baseline recording in one rat. LFP was extracted from an electrode array in the visual cortex, and color indicates power, normalized to the maximum value at each time point. *Top*: Colored boxes indicate the rat's behavioral state over the same time course as the LFP spectrogram. Behavior was coded using LFP, EMG, and video data. Blue = Non-REM Sleep; green = REM Sleep; yellow = Quiet Wake; orange = Active Wake. (*F*) Average power in each of three LFP frequency bands in the 8 h after subcutaneous CNO injections, normalized to time- and circadian-matched baseline periods on recording days without CNO injections; each data point represents one animal. The dashed line represents baseline. One sample t test comparing normalized values to no change, with Bonferroni correction for multiple comparisons. Delta = 0.5 to 4 Hz; P = 0.0075. Theta = 6 to 8 Hz; P = 0.11. Alpha = 9 to 15 Hz; P = 0.035. (*G*) Percent time spent in each of four behavioral states in the 8 h after subcutaneous CNO injections, normalized to time- and circadian-matched baseline periods before the CNO injections. As above, each data point represents one animal (n = 6), and the dashed line represents baseline. 1 sample t test comparing each normalized value to no change, with Bonferroni correction for multiple comparisons. REM = Rapid Eye Movement Sleep; P = 0.047. NREM = Non-REM Sleep; P = 1. AW = Active Wake; P = 1. QW = Quiet Wake; P = 1. *F* and *G*: N = 6 ChAT-cre rats, all with Hm4di virus injections into the HDB.

to one hemisphere of V1 and gave rats ad libitum access to CNO drinking water (0.05 mg/mL) for 48 h prior to slice electrophysiology, then targeted infected L2/3 pyramidal neurons for whole-cell voltage-clamp recordings (Fig. 2 *A*–*C*). We first confirmed that activity suppression with Hm4di + CNO indeed induced synaptic scaling up in L2/3 pyramids: Hm4di$^+$ neurons had significantly larger miniature excitatory post-synaptic currents (mEPSCs) than Hm4di$^-$ neurons (CNO only, 10.6 ± 0.1 pA vs. V1 Hm4di + CNO, 11.2 ± 0.1). In contrast, when the HDB was inhibited at the same time as V1 (by expressing Cre-dependent Hm4di in HDB ACh neurons), V1 activity suppression no longer increased mEPSC amplitude (Fig. 2*D*; HDB ACh Hm4di + CNO, 11.0 ± 0.1 vs. V1 + HDB ACh Hm4di + CNO, 11.4 ± 0.2). In comparing all four conditions we noticed that HDB ACh inhibition had slightly larger mEPSCs than the CNO-only condition (Fig. 2*D*, V1 + HDB ACh Hm4di + CNO significantly different from CNO only). There was no significant difference in mEPSC frequency in any group (Fig. 2*E*), and only subtle differences in passive properties (*SI Appendix*, Table S2). Thus, HDB ACh inhibition alone causes a small increase in mEPSC amplitude in L2/3 pyramidal neurons and prevents further scaling up.

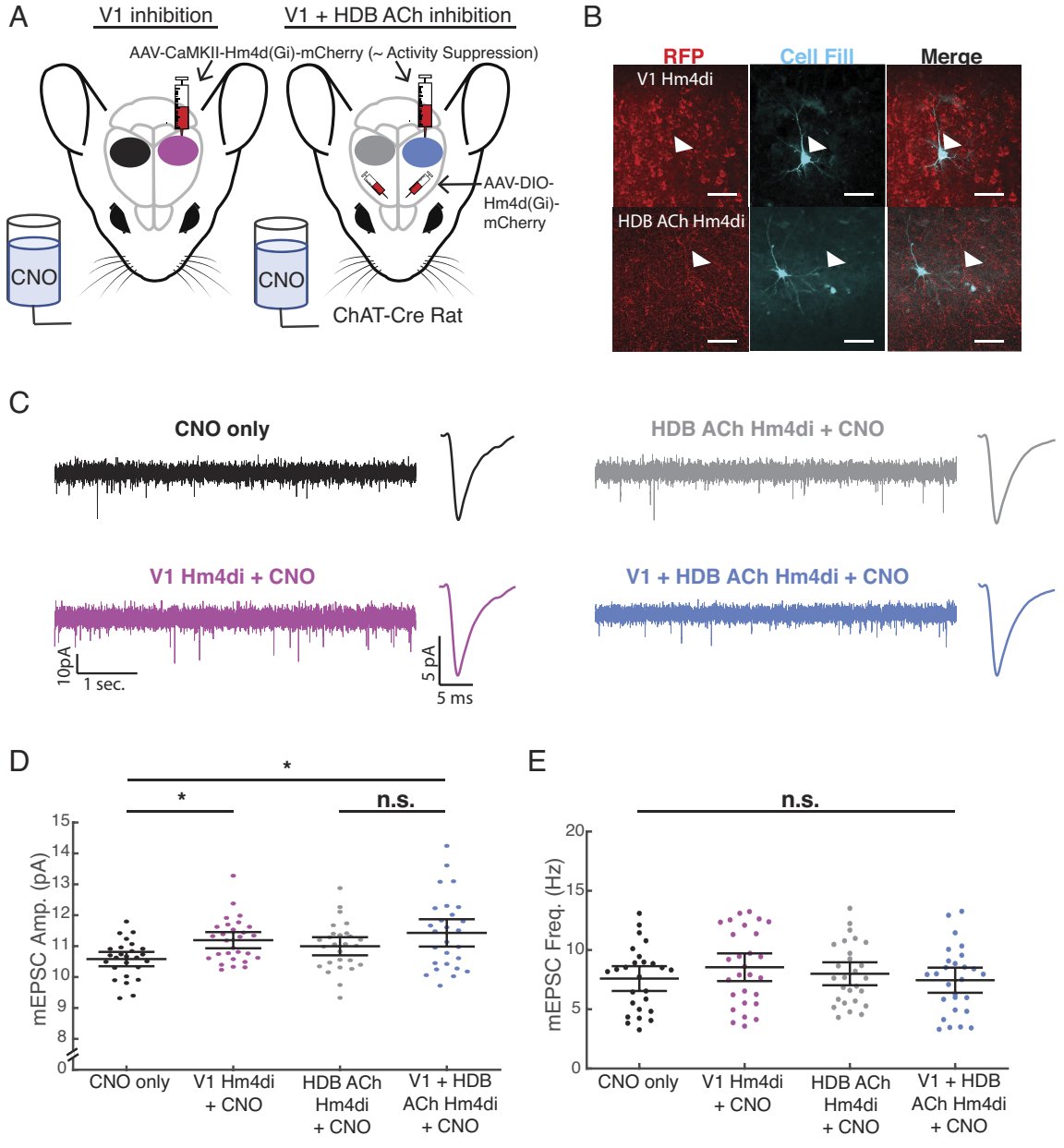

Fig. 2. Inhibition of HDB ACh neurons impairs synaptic scaling. (*A*) Schematic of experimental design. Virus expressing Hm4di driven by a CaMKII promoter was injected unilaterally in V1m of each rat, with the other hemisphere serving as a within-animal control. In one set of ChAT-cre rats, virus expressing Cre-dependent Hm4di was also injected bilaterally in the HDB. All animals had access to ad libitum water with CNO for 48 h prior to killing for ex vivo electrophysiology. (*B*) Example images of Hm4di expression and biocytin cell fill from recorded V1m L2/3 pyramidal cells. *Top*: Hm4di expression (RFP) driven by CaMKII in the visual cortex; the white arrowhead indicates the filled Hm4di+ neuron. *Bottom*: The white arrowhead indicates Hm4di+ projections (RFP) in V1m near a recorded cell; image taken from control hemisphere of an animal that received Cre-dependent Hm4di injections into the HDB. (Scale bar, 50 μm.) (*C*) Representative mEPSC traces from each experimental group. (*D* and *E*) mEPSC amplitudes (*D*) and frequencies (*E*) of all recorded cells in each experimental group. Black lines indicate mean ± SEM. CNO only: 26 cells from 9 animals; V1 Hm4di + CNO: 28 cells from 9 animals; HDB ACh Hm4di + CNO: 27 cells from 6 animals; V1 Hm4di + HDB ACh Hm4di + CNO: 27 cells from 6 animals. *D*: Kruskal–Wallis test $P = 0.016$ with Tukey-Kramer post hoc. CNO only vs. V1 Hm4di + CNO: $P = 0.038$; CNO only vs. HDB ACh Hm4di + CNO: $P = 0.28$; CNO only vs. V1 + HDB ACh Hm4di + CNO: $P = 0.019$; V1 Hm4di + CNO vs. HDB ACh Hm4di + CNO: $P = 0.82$; V1 Hm4di + CNO vs. V1 + HDB ACh Hm4di + CNO: $P = 0.99$; HDB ACh Hm4di + CNO vs. V1 + HDB ACh Hm4di + CNO: $P = 0.671$. *E*: Kruskal–Wallis test $P = 0.59$.

HDB ACh Inhibition Flips the Sign of Intrinsic Plasticity. We next examined how HDB ACh inhibition affects intrinsic excitability. We used the same dual inhibition of V1 and HDB paradigm as above (Fig. 3*A*), except we recorded from infected L2/3 pyramidal neurons in current clamp in the presence of synaptic blockers and constructed FI curves by injecting a series of DC current steps to elicit spikes (Fig. 3 *B* and *C*). DREADDs-mediated inhibition of V1 alone caused a small increase in intrinsic excitability compared to no treatment; this was apparent at higher current injections and included significant increase in the slope of the linear portion of the f–I curves (Fig. 3 *B* and *E*, "V1 Empty Vector + CNO" vs. "V1 Hm4di + CNO" conditions). A second measure of IHP, the area under the FI curve (Fig. 3*D*) was not significantly increased. Remarkably, simultaneous inhibition of HDB ACh neurons and V1 induced a dramatic decrease in intrinsic excitability, characterized by a rightward and downward shift in the FI curve (Fig. 3*C*), a significant decrease in the slope of the linear portion of the FI curve (Fig. 3*E*), and a significant decrease in the area under the FI curve (Fig. 3*D*). This decrease in excitability was accompanied by a significant increase in rheobase (Fig. 3*F*), with no significant change in input resistance or other passive properties for any condition (Fig. 3*G* and *SI Appendix*, Table S3). These data show that HDB ACh inhibition can flip the sign of intrinsic plasticity during activity deprivation from a compensatory (homeostatic) increase, to an anti-homeostatic decrease. Thus, HDB ACh activity plays a critical role in determining the sign of intrinsic plasticity.

Knockdown of M1 ACh Receptors In Vitro and In Vivo. Inhibition of HDB ACh neurons induces a striking sign-change in L2/3 pyramidal neuron intrinsic plasticity, leading us to wonder if this effect is mediated via direct release of ACh onto L2/3 pyramidal neurons. The M1 ACh receptor is a Gq-coupled metabotropic receptor that is highly expressed in the rodent visual cortex, especially on somas and dendrites of L2/3 pyramidal neurons (32–34). We therefore targeted M1 for knockdown by generating a short hairpin plasmid targeting the 3′UTR of rat M1 as well as YFP to visualize infected neurons. When this plasmid was transfected into cultured cortical neurons, we found a significant reduction in M1 AChR protein compared to neurons transfected with an empty vector, as assessed by immunohistochemistry (Fig. 4 *A*–*C*). We then packaged the shRNA into an AAV9 viral vector and targeted V1 for virus injections prior to immunohistochemistry or electrophysiology. In V1 NeuN selectively labels pyramidal neurons (35, 36); we observed robust expression in both $NeuN^+$ and $NeuN^-$ neurons, with about 62 ± 7% of YFP+ cells expressing NeuN (Fig. 4*D*). This indicates that our shRNA likely infected both pyramidal neurons and interneurons, but we restricted our recordings in subsequent experiments to YFP+ L2/3 pyramidal neurons as above. To assess the functional efficacy of M1 knockdown we obtained whole-cell current clamp recordings and activated ACh receptors by washing in carbachol (CCh), a stable ACh analog, while injecting a series of small depolarizing and hyperpolarizing current steps to measure changes in firing and passive properties (Fig. 4*E*). Consistent with previous reports of M1-mediated CCh modulation (37, 38), CCh wash-in increased the magnitude of the after-depolarization potential (ADP); this effect reversed upon CCh washout and was abolished by M1 knockdown (Fig. 4 *E* and *F*), as was the ability of CCh to increase firing (without M1 knockdown, control vs. CCh, $P = 0.0016$; with M1 knockdown, $P = 0.12$). These data show that we can effectively knock down M1 ACh receptor expression in V1 and that in L2/3 pyramidal neurons, this receptor mediates most of the acute postsynaptic response to CCh application.

Knockdown of the M1 Receptor in V1 Phenocopies the Effect of HDB ACh Inhibition on Intrinsic Plasticity. If inhibiting HDB ACh neurons flips the sign of intrinsic plasticity by reducing cholinergic modulation of L2/3 pyramidal neurons, then knocking down the M1 receptor in L2/3 neurons might phenocopy this effect. To test this, we virally expressed in V1 either our M1 shRNA alone or the M1 shRNA + CaMKII-Hm4di (Fig. 5*A*). Animals then received CNO in their drinking water for 24 h prior to ex vivo recordings from infected L2/3 pyramidal neurons to measure intrinsic excitability; experiments were performed 6 to 10 d after shRNA delivery. Similar to the combination of HDB ACh inhibition and V1 activity suppression (Fig. 3), the combination of M1 knockdown and V1 activity suppression caused a rightward and downward shift in the FI curve compared to M1 knockdown alone (Fig. 5 *B* and *C*). As for HDB ACh inhibition, this was accompanied by a significant decrease in area under the FI curve (Fig. 5*D*) and increase in rheobase (Fig. 5*F*). This suggests HDB ACh activity exerts its effects on intrinsic plasticity through direct activation of M1 ACh receptors within V1.

Viral knockdown of M1 for 6 to 10 d induced a substantial increase in input resistance in infected L2/3 pyramidal neurons with or without Hm4Di expression, consistent with a decrease in resting conductance (Fig. 5*G*). Interestingly, after longer M1 knockdown (14 to 19 d), this increase in input resistance reversed (*SI Appendix*, Table S4), and V1 activity suppression no longer reduced intrinsic excitability ($P = 0.73$). This suggests that prolonged loss of M1 induces compensatory changes in L2/3 neurons.

HDB ACh Inhibition Prevents Upward FRH. During monocular deprivation (MD), firing rates in V1 first decrease (MD 1–2) and are then slowly restored to baseline during MD 3–4 (4, 7, 8, 12), a homeostatic process that depends on synaptic scaling and intrinsic homeostatic plasticity in L2/3 pyramidal neurons (7, 9, 12). We therefore wondered whether HDB ACh neuron activity is necessary for the in vivo expression of upward FRH. To test this, we obtained continuous extracellular single unit recordings from V1m of freely behaving rats as described (4, 8), performed MD, and then inhibited HDB ACh neurons by administering CNO when firing rates normally recover during MD 3 and MD 4 (Fig. 6*A*). First, we replicated our previous demonstrations of upward FRH in two "CNO-only" control animals, one with no viral injection into the HDB and one where the injection failed and DREADDs expression was minimal (12% of ChAT+ neurons in HDB were RFP+, vs. 88, 85, 83, and 75% in animals in the "Hm4di+CNO" group; Fig. 6*B*). Consistent with previous work, in the CNO-only condition, regular spiking V1 neurons had a broad distribution of baseline firing rates, firing was depressed across the distribution on MD2, and firing then returned to baseline by MD 4 (Example neuron, Fig. 6*D* lower trace; all data, Fig. 6*E*). In contrast, inhibition of HDB ACh neurons during MD 3-4 completely prevented the normal recovery of firing rates; in this condition, firing rates on average fell even further below baseline on MD4 (example neuron Fig. 6*D* upper trace, all data Fig. 6*F*; $n = 4$ animals). Importantly, we found that HDB ACh inhibition had no acute effect on V1m firing rates (Fig. 6*C*). Thus, upward FRH in V1m is critically dependent on the activity of HDB ACh neurons.

Discussion

Upward FRH during sensory deprivation in V1 is gated by behavioral state and occurs exclusively during active waking states, but how this gating is achieved is unknown. Here, we show that cholinergic projections to V1 from the HDB of the basal forebrain are critical for the proper expression of two cellular homeostatic

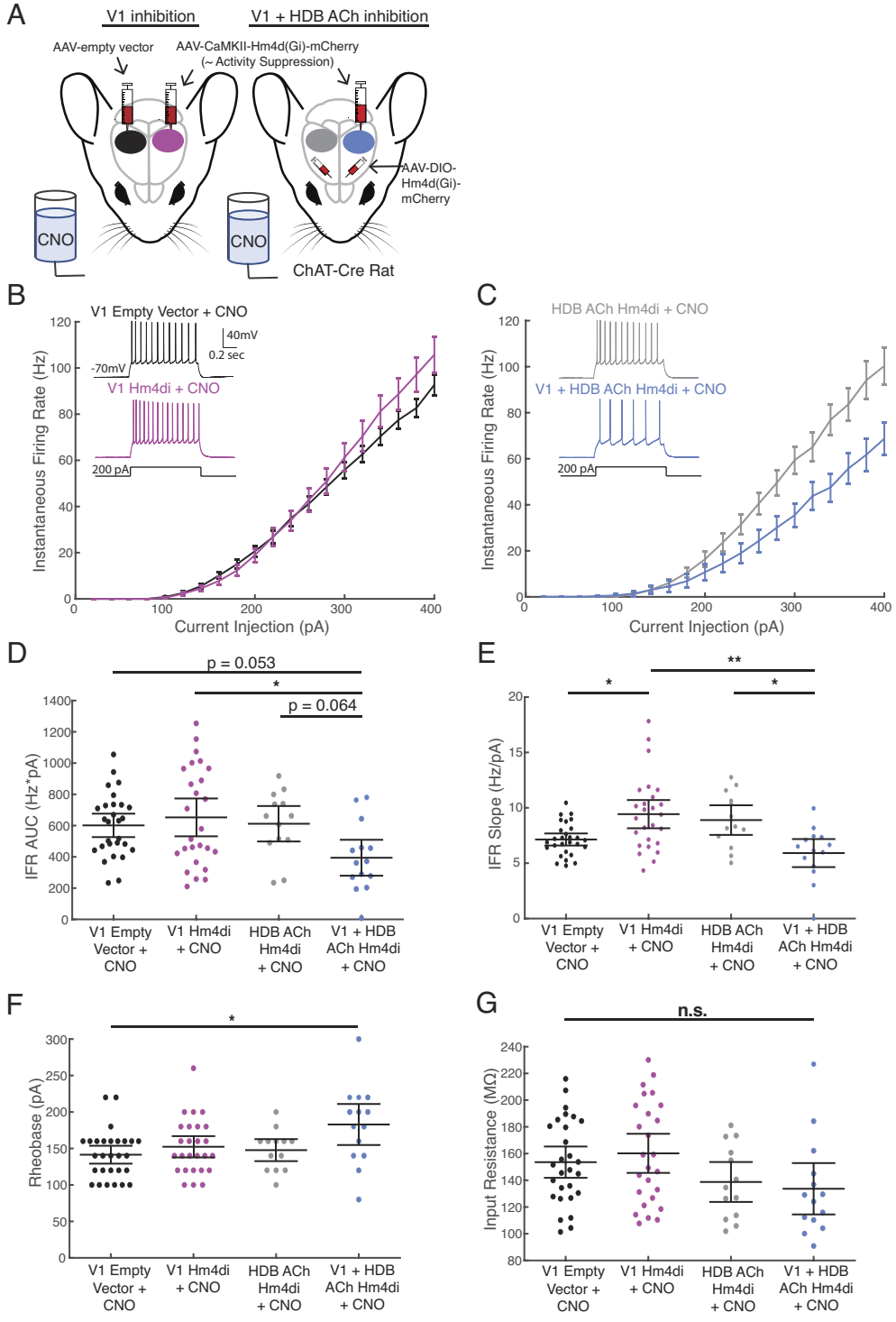

Fig. 3. HDB ACh inhibition during activity suppression in V1 changes the sign of intrinsic plasticity. (*A*) Schematic of experimental design. All animals had access to ad libitum water with CNO for 24 h prior to killing for ex vivo electrophysiology. (*B*) Firing rate–current injection (f–I) curves for experimental conditions without HDB ACh inhibition. The *y*-axis indicates mean instantaneous firing rate. *Inset*: Representative recordings from a V1m L2/3 pyramidal neuron from each condition plotted here, evoked by 200 pA current injection. (*C*) f–I curves for experimental conditions with HDB ACh inhibition. The y axis indicates mean instantaneous firing rate. *Inset*: Representative recordings from a V1m L2/3 pyramidal neuron from each condition plotted here, evoked by 200 pA current injection. (*D*) Quantification of the area under each f–I curve, calculated individually for each neuron. Black lines indicate mean ± SEM. Kruskal–Wallis test $P = 0.025$ with Tukey-Kramer post hoc. V1 empty vector + CNO vs. V1 Hm4di + CNO: $P = 0.98$; V1 empty vector vs. HDB ACh Hm4di + CNO = 0.98; V1 empty vector + CNO vs. V1 + HDB ACh Hm4di + CNO = 0.053; V1 Hm4di + CNO vs. HDB ACh Hm4di + CNO = 1; V1 Hm4di + CNO vs. V1 + HDB ACh Hm4di + CNO: $P = 0.027$; HDB ACh Hm4di + CNO vs. V1 + HDB ACh Hm4di + CNO: $P = 0.064$. (*E*) Quantification of the slope of the line fitted to the linear portion of each f–I curve, calculated individually for each neuron. Black lines indicate mean ± SEM. Kruskal–Wallis test $P = 0.00084$ with Tukey-Kramer post hoc. V1 empty vector + CNO vs. V1 Hm4di + CNO: $P = 0.033$; V1 empty vector vs. HDB ACh Hm4di + CNO = 0.16; V1 empty vector + CNO vs. V1 + HDB ACh Hm4di + CNO = 0.60; V1 Hm4di + CNO vs. HDB ACh Hm4di + CNO = 1; V1 Hm4di + CNO vs. V1 + HDB ACh Hm4di + CNO: $P = 0.0030$; HDB ACh Hm4di + CNO vs. V1 + HDB ACh Hm4di + CNO: $P = 0.021$. (*F*) Rheobase for each recorded cell. Black lines indicate mean ± SEM. Kruskal–Wallis test $P = 0.039$ with Tukey-Kramer post hoc. V1 empty vector + CNO vs. V1 Hm4di + CNO: $P = 0.75$; V1 empty vector vs. HDB ACh Hm4di + CNO = 0.92; V1 empty vector + CNO vs. V1 + HDB ACh Hm4di + CNO = 0.021; V1 Hm4di + CNO vs. HDB ACh Hm4di + CNO = 1; V1 Hm4di + CNO vs. V1 + HDB ACh Hm4di + CNO: $P = 0.18$; HDB ACh Hm4di + CNO vs. V1 + HDB ACh Hm4di + CNO: $P = 0.24$. (*G*) Input resistance for each recorded cell. Kruskal–Wallis test: $P = 0.063$. Sample size for all plots: V1 Empty Vector + CNO: $n = 28$ cells from 7 animals; V1 Hm4di + CNO: $n = 26$ cells from 7 animals; HDB ACh Hm4di + CNO: $n = 13$ cells from 4 animals; V1 Hm4di + HDB ACh Hm4di + CNO: $n = 14$ cells from 4 animals.

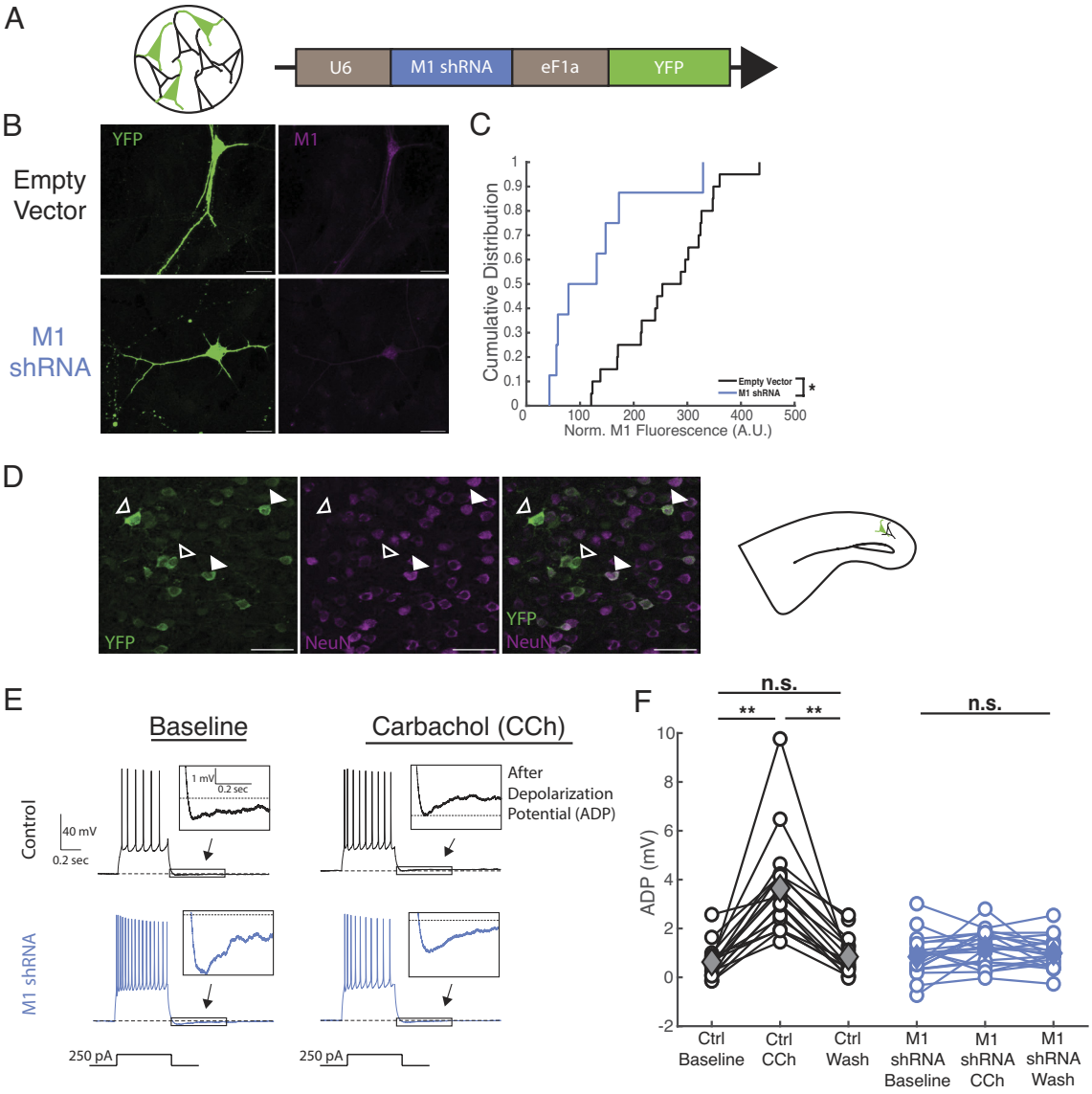

Fig. 4. Knockdown of M1 ACh receptors in vitro and in vivo. (*A*) Schematic indicating experimental system (neuronal cultures) and plasmid containing shRNA targeting M1 ACh receptors (M1 shRNA) used in *B* and *C*. (*B*) Example images of cultured neurons transfected with an empty vector plasmid (*Top*) or a plasmid containing M1 shRNA (*Bottom*). Green = YFP; magenta = M1 ACh receptor. (Scale bar, 20 μm.) (*C*) Cumulative distribution curves of M1 fluorescence intensity in somas of cultured neurons transfected with an empty vector (black) or M1 shRNA (blue); the M1 shRNA curve is significantly left shifted, indicating a reduction in M1 fluorescence intensity compared to empty vector. Cultures were fixed and stained after 3 d of transfection. Fluorescence intensities for each cell were normalized to the average fluorescence intensity of empty vector neurons in the corresponding group of cultures to account for any dissection-related differences. Kolmogorov–Smirnov test $P = 0.012$. Empty vector: $n = 20$ cells from 4 dissections, m1 shRNA: $n = 8$ cells from 3 dissections. (*D*) *Right*: schematic indicating ex vivo slice preparation for *D–G*. *Left*: Example image of an AAV9-M1 shRNA-YFP injection in V1m L2/3. 62 ± 7% of YFP+ neurons were also NeuN+. Open arrowheads denote YFP+ cells, indicating expression of our shRNA, that did not express NeuN. Closed arrowheads denote YFP+ cells that also expressed NeuN. Green = YFP; magenta = NeuN. (Scale bar, 50 μm.) (*E*) Control or knockdown neurons were recorded for several minutes of baseline in regular ACSF with synaptic blockers, followed by 10 min of Carbachol (CCh) wash-in and 10 more minutes of CCh wash-out. Representative traces from a control and a knockdown neuron in response to 250 pA of injected current, under baseline conditions (*Left*) and in the presence of CCh (*Right*). Note that the control cell shows an increased firing rate and presence of an after-depolarization potential (ADP) in CCh compared to baseline, while the M1 shRNA cell does not show ADP in the presence of CCh and shows a slight decrease in firing rate, likely due to the long recording time. (*F*) Quantification of ADP for each recorded neuron at baseline, at the end of the CCh wash-in, and at the end of the CCh wash-out (open circles). The solid diamonds indicate the mean. Control cells: $n = 16$ cells from 4 animals. M1 shRNA cells: $n = 20$ cells from 4 animals. Wilcoxon sign-rank test with Bonferroni correction. Ctrl baseline vs. Ctrl CCh: $P = 0.0013$; Ctrl CCh vs. Ctrl Wash: $P = 0.0013$; Ctrl baseline vs. Ctrl Wash: $P = 1$; M1 baseline vs. M1 CCh: 0.17; M1 CCh vs. M1 wash: 1; M1 baseline vs. M1 wash: 0.84.

plasticity mechanisms known to contribute to upward FRH and find that this effect is mediated at least in part through activation of M1 ACh receptors within V1. Further, we find that inhibiting HDB ACh neurons during prolonged visual deprivation prevents upward FRH. Together, our data show that wake-active cholinergic inputs to V1 are a critical mediator of upward homeostatic compensation and suggest more broadly that the control of neuromodulatory tone enables particular vigilance states to gate the expression of homeostatic plasticity within neocortical circuits.

A salient difference between AW (when upward FRH is robustly induced) and QW (when it is absent) is the activity of neuromodulatory inputs. Specifically, cholinergic and noradrenergic inputs are most active during AW and contribute to the highly desynchronized cortical activity typical of this state (15, 39). Two considerations made ACh a promising starting point for exploring neuromodulatory gating of homeostatatic plasticity. First, the target specificity of BF ACh sub-regions (24) allowed us to target HBD inputs to V1 with greater specificity than possible for

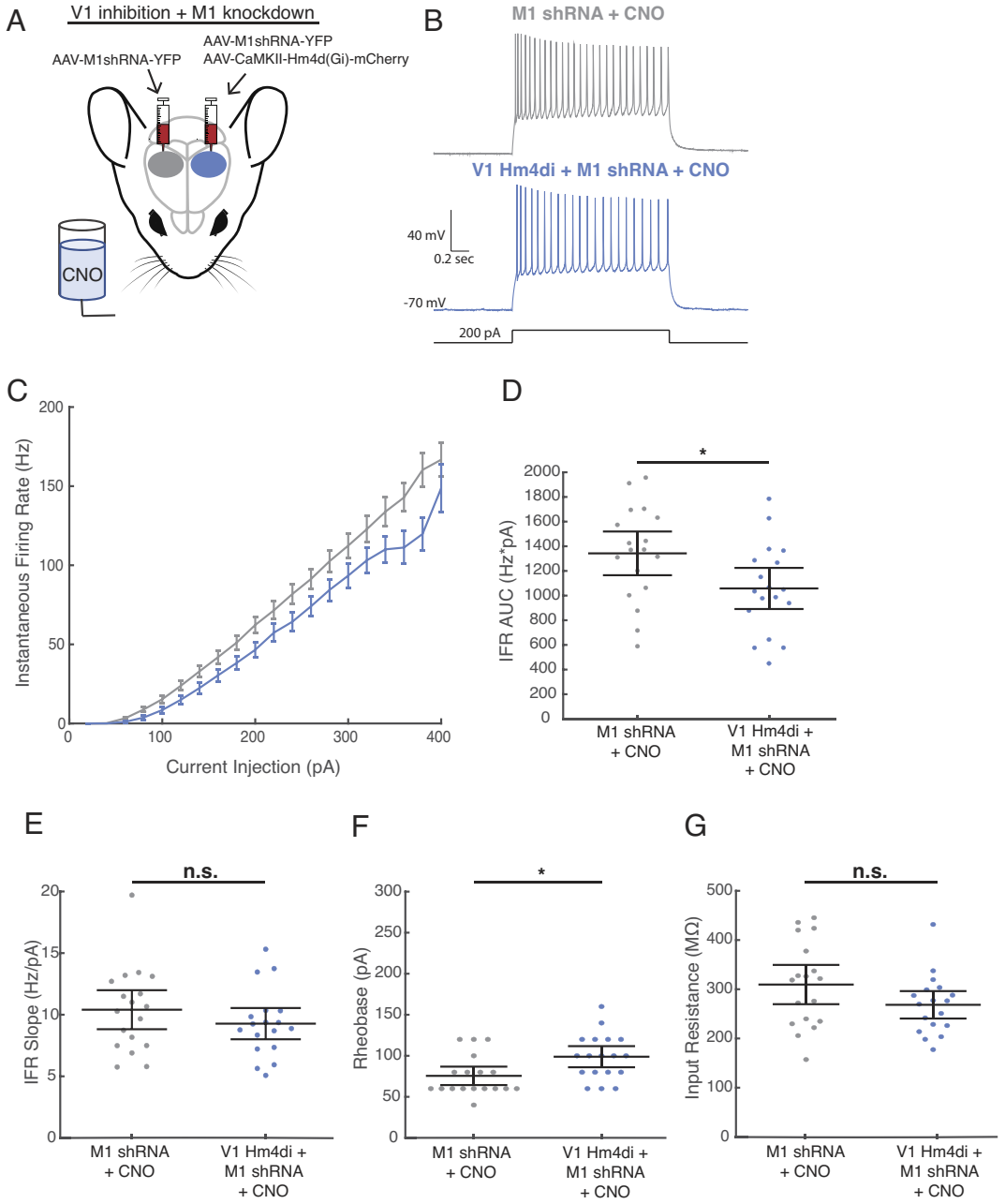

Fig. 5. Activity suppression in V1 during M1 Knockdown reduces intrinsic excitability. (*A*) Schematic of the experimental design. All animals had access to ad libitum water with CNO for 24 h prior to killing for ex vivo electrophysiology. (*B*) Representative recordings from V1m L2/3 pyramidal neurons from each experimental group evoked by 200 pA current injection. (*C*) f–I curves for each experimental condition. The *y*-axis indicates instantaneous firing rate. (*D*) Quantification of the area under each f–I curve, calculated individually for each neuron. Black lines indicate mean ± SEM. Wilcoxon rank-sum test: $P = 0.024$. (*E*) Quantification of the slope of the line fitted to the linear portion of each f–I curve, calculated individually for each neuron. Black lines indicate mean ± SEM. Wilcoxon rank-sum test: $P = 0.35$. (*F*) Rheobase for each recorded cell. Black lines indicate mean ± SEM. Wilcoxon rank-sum test: $P = 0.013$. (*G*) Input resistance for each recorded cell displayed in the rest of the figure. Note that input resistance for both M1 knockdown groups is substantially higher than for all cells in previous experiments (Fig. 3 and *SI Appendix*, Tables S2–S4). Black lines indicate mean ± SEM. Wilcoxon rank-sum test: 0.14. Sample size for all plots: M1 shRNA: 18 cells from 5 animals; M1 shRNA + V1 Hm4di: 18 cells from 5 animals.

noradrenergic inputs (24). Second, there is an extensive literature on the role of cholinergic modulation in experience-dependent plasticity in the neocortex (18, 20, 21, 40). Cholinergic modulation causes long-term enhancement of visual cortex responses to salient stimuli (20, 21); facilitates some forms of long-term depression (41, 42); and can enhance ocular dominance plasticity within V1 (18), which in turn relies on upward homeostatic plasticity for its full expression (3). Cholinergic modulation has a diversity of effects on target neurons due to multiple receptor subtypes and modes of release (33, 37, 43, 44). Our results demonstrate that HDB ACh activity is necessary for the induction of upward FRH during visual deprivation and acts in part through M1 receptors onto L2/3 pyramidal neurons within V1. Our data leave open the possibility that other ACh receptors on other cell types also contribute to the gating of FRH and that other neuromodulatory inputs [such as noradrenergic inputs; (45)] could act synergistically with cholinergic inputs during the normal induction of FRH. Such cooperativity might provide a mechanism by which specific constellations of cellular plasticity mechanisms could be brought on or offline during distinct brain states.

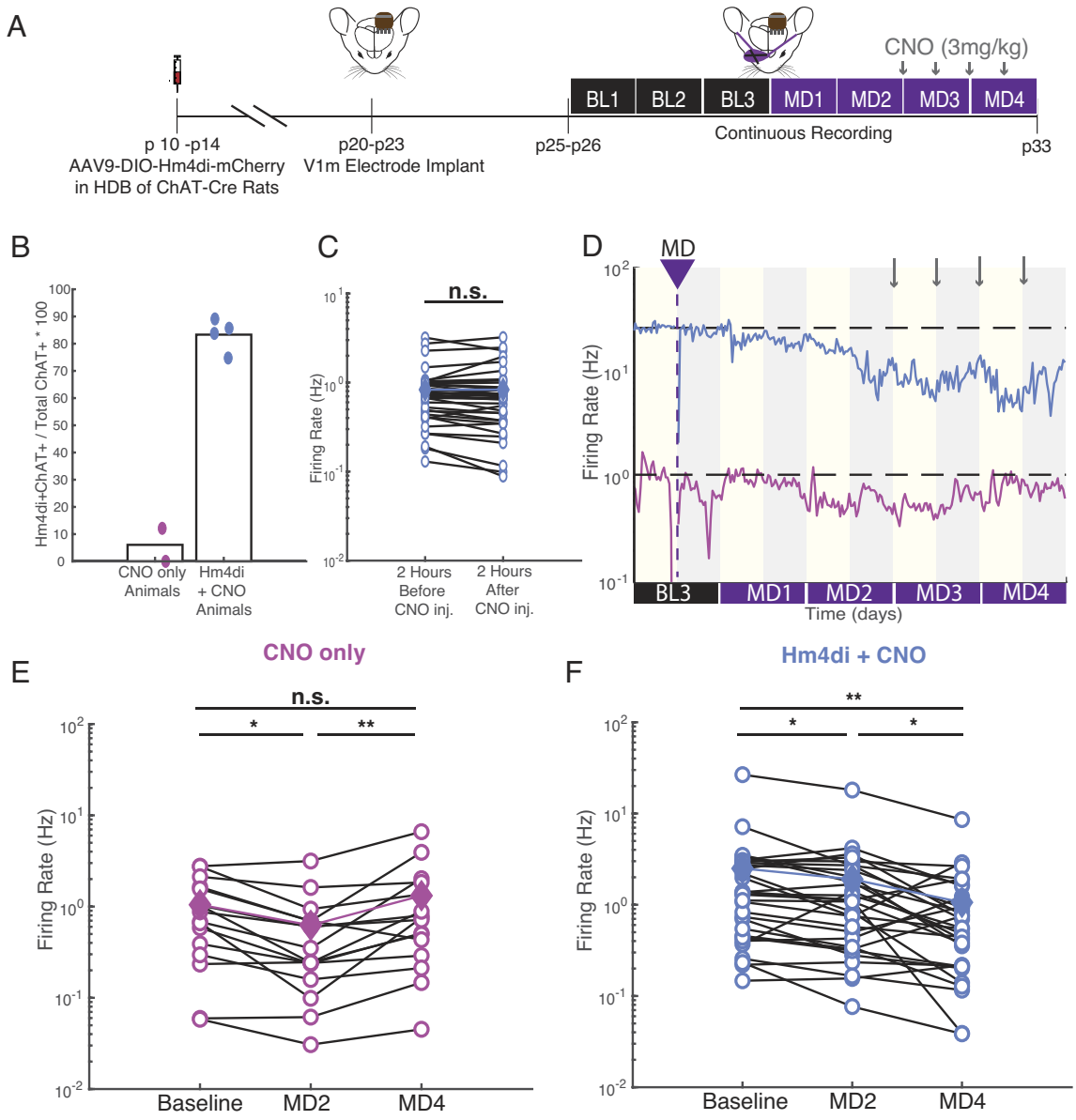

Fig. 6. HDB ACh inhibition prevents upward FRH. (*A*) Experimental timeline. All but one animal underwent virus injection surgery at or before p14. After at least 1 wk of recovery, animals underwent electrode array implant in the monocular visual cortex. After at least 3 more days of recovery, continuous recording began and lasted for 7 d. All experiments were complete before p33 and thus occurred within the classical visual system critical period. During the dark period on the third day of baseline, monocular deprivation (MD) was performed on the eye contralateral to the electrode implant. During the third and fourth days of MD, animals received four total subcutaneous CNO injections, one every 12 h starting at ZT0 on MD3. (*B*) Quantification of virus expression in ChAT+ cells in the horizontal diagonal band (HDB) of all animals used in these in vivo experiments. One animal that underwent virus injection showed very little virus expression (12% ChAT+ neurons in HDB were also mCherry+), so we included that animal in the CNO-only cohort. The CNO-only cohort also included another animal that did not receive any virus injection. In contrast, the four animals that were included in the Hm4di + CNO cohort had 75, 88, 85, and 83% of ChAT+ neurons in the HDB also mCherry+. (*C*) Inhibition of HDB ACh neurons does not acutely change firing rates of V1m regular spiking units. The firing rates of neurons from animals in the Hm4di + CNO cohort were indistinguishable in the 2 h immediately preceding each CNO injection compared to the 2 h immediately after each CNO injection. Empty circles each represent one cell; solid diamonds and colored line represent the mean firing rate at each time point. Mean FR before = 0.83 Hz, Mean FR after = 0.83 Hz. Median FR before = 0.70 Hz, Median FR after = 0.68 Hz. $N = 37$ cells from 4 animals. Wilcoxon sign-rank test; before vs. after: $P = 0.36$. (*D*) Firing rate traces of two example deprived cells over the course of the monocular deprivation, one from the Hm4di + CNO cohort, and one from a CNO-only animal. (*E* and *F*) Ladder plot showing the activity of each deprived cell in the CNO-only (*E*) and Hm4di + CNO (*F*) cohort averaged over a 12-h period on baseline day 3, MD2, and MD4 in the open circles. The solid diamonds show the mean firing rate of all cells at each time point. The activity of deprived cells in *E* is significantly lower than baseline on MD2, but back up to baseline levels on MD4, while the activity of deprived cells in *F* is significantly lower than baseline on MD2 and still significantly lower than baseline on MD4. $N = 16$ cells from 2 animals (*E*) and 30 cells from 4 animals (*F*). Wilcoxon sign-rank test with Bonferroni correction for multiple comparisons. E: Baseline vs. MD2: $P = 0.011$; MD2 vs. MD4: $P = 0.007$; Baseline vs. MD4: $P = 1$. F: Baseline vs. MD2: $P = 0.040$; MD2 vs. MD4: $P = 0.010$; Baseline vs. MD4: $P = 0.003$.

Reducing HDB ACh modulation impaired the expression of two cellular forms of plasticity known to contribute to upward FRH in L2/3 pyramidal neurons: synaptic scaling up and intrinsic homeostatic plasticity (4, 9). Inhibiting HDB ACh activity alone induced a small increase in baseline mEPSC amplitude and prevented direct activity suppression within V1 from further increasing postsynaptic strength. The baseline effect on mEPSC amplitude makes it difficult to determine whether this represents a simple block or partial occlusion/partial block of synaptic scaling up; regardless, these data show that HDB ACh activity is important for the normal expression of synaptic scaling up in L2/3 pyramidal neurons.

Intrinsic plasticity contributes to homeostatic network compensation in many cell types within the sensory cortex (46, 47), and the most dramatic cellular effect of HDB ACh inhibition was on the induction of intrinsic plasticity. Activity suppression in V1 produced a homeostatic increase in the intrinsic excitability of L2/3 pyramidal neurons under baseline conditions as expected, although this effect was smaller than that reported using the same approach in mouse V1 L2/3 neurons, possibly due to developmental regulation of this form of plasticity (11). However, when HDB ACh neurons were inhibited, this same manipulation produced a dramatic decrease in intrinsic excitability. Importantly, inhibiting HDB ACh neurons alone had no effect on baseline intrinsic excitability, indicating that it is the conjunction of activity suppression and loss of HDB ACh input that drives this anti-homeostatic decrease in the input–output function. This is reminiscent of the effects of visual deprivation on the intrinsic excitability of L5 pyramidal neurons, where brief MD in V1m drives a reduction in intrinsic excitability during the critical period, but not before or after (48, 49). Whether this developmental regulation of intrinsic plasticity in L5 pyramidal neurons is tied to changes in cholinergic modulation is unknown. Notably, the decrease in L2/3 pyramidal neuron intrinsic excitability induced by conjoint reduction of cholinergic inputs and V1 activity would be expected to reduce rather than boost firing, making this change in sign of intrinsic plasticity a likely contributor to the lack of upward FRH during HDB ACh inhibition.

HDB ACh axons project to and terminate within V1 [(24); Fig. 1], but also have other targets, including the hippocampus and other cell types within the BF (17, 50, 51). To determine whether inhibition of HDB ACh neurons exerts their influence on intrinsic plasticity by directly activating ACh receptors in V1, we knocked down expression of the abundant M1 receptor and found that—when combined with activity suppression in V1—this manipulation also induced a significant decrease in the intrinsic excitability of L2/3 pyramidal neurons. The effect of M1 knockdown was not as dramatic as HDB ACh inhibition: This could be because the knockdown was incomplete; alternatively, there might be additional targets of HDB ACh neurons that contribute to the activity-dependent drop in intrinsic excitability; finally, more prolonged M1 knockdown (>2 wk) appears to induce a compensatory response that may be partially evident at the time point used here (6 to 10 d of knockdown). Regardless, these data show that HDB ACh activity enables homeostatic intrinsic plasticity of L2/3 pyramidal neurons at least in part through direct ACh release and activation of M1 ACh receptors within V1.

An important open question is what intracellular signals detect the conjunction of activity levels and M1 activation to determine the sign of intrinsic plasticity. Further, while we show that the activity of basal forebrain cholinergic neurons is necessary for upward FRH, the ability of sleep states to gate downward FRH likely requires more than the simple absence of cholinergic modulation, because it occurs equally across NREM and REM sleep (8), which have very different levels of BF activity (22). Each brain state activates a unique set of modulatory influences on neocortical circuits, and it seems likely that these in turn recruit specific constellations of cellular homeostatic mechanisms to enable neocortical circuits to undergo upward or downward FRH.

Materials and Methods

Animals. Experiments were performed on Long Evans rats [both wild-type (WT) and transgenic rat lines] of both sexes. All ChAT-Cre transgenic rats (52) were bred as heterozygotes and continuously back-crossed with WT Long Evans rats. Experiments were carried out between postnatal day 24 (P24) and P32, during the classical visual system critical period. All animals were treated in accordance with Brandeis Institutional Biosafety Committee and Institutional Animal Care and Use Committee protocols. Pups were weaned at P21 and housed (12 h L/D cycle, ad libitum access to food and water) with at least one littermate except for post-surgical recovery when experiments required single housing. The number of animals and neurons for each experiment is given in the figure legends, and individual data points represent neurons, except in Fig. 1, where they represent animals.

Virus Injection. Virus injections were performed on juvenile rats on a stereotaxic apparatus under isoflurane anesthesia. V1m or the horizontal diagonal band (HDB) region of the basal forebrain (2 locations per hemisphere) were targeted using the following stereotaxic coordinates determined from ref. 53: for V1m, 1) A/P −7.3 to −6.9 mm; M/L ± 2 to 3 mm; D/V 0.8 to 0.4 mm; and 2) A/P −6.7 mm; M/L ± 2.8 to 3 mm; D/V 0.8 to 0.4 mm; for HDB, 1) A/P 0.3 mm; M/L ± 0.3 to 0.5 mm; D/V 8.5 mm; and (2) A/P −0.2 to −0.3 mm; M/L ± 2 mm; D/V 9 mm for a bregma–lambda distance of 9 mm. 200 to 300 nL of virus were delivered into the targeted area via a micropipette.

Electrode Implants, Monocular Derivation, Continuous Recordings, and Behavioral State Scoring. Rats were implanted with electrode arrays, and continuous single-unit recordings, spike extraction, clustering, and sorting were performed using our previously described pipeline (4, 7, 8). Behavioral state scoring was performed as previously described (4, 8), except animal movement was tracked from video recordings using DeepLabCut (54). Additional details can be found in supplemental methods.

Drug Administration. For subcutaneous injections, water-soluble CNO (Hello Bio) was dissolved in 0.9% sterile saline to reach the desired concentration (1 mg/mL). For drinking water CNO administration, CNO was dissolved in water to reach the desired concentration (0.05 mg/mL), and 10 mM saccharine chloride was added to the solution before giving the solution to the animals. For DREADD (Hm4di) activation, CNO was administered via subcutaneous injections at a dose of 3 mg/kg every 12 h or via drinking water ad libitum. When administered via drinking water, animals drank 15 to 20 mL per day to reach a dose of 10 to 15 mg/kg over the course of 24 h.

M1 shRNA Generation. The shRNA sequence (5′-GAACCCACTGCATCTACATTT-3′) used for M1 knockdown was designed with the TRC algorithm (Broad Institute) and cloned into the pAAV-shRNA-ctrl vector from Addgene. pAAV-shRNA-ctrl was used as the empty vector plasmid in Fig. 5. Our M1 shRNA plasmid was packaged in AAV9 viral vectors by Duke Viral Core. A modified version of the pAAV-shRNA-ctrl plasmid (eYFP was replaced with eGFP) had already been packaged in an AAV9 viral vector by a previous member of the lab, Lauren Tereshko, and this was used for empty vector in vivo viral injections.

Statistical Analyses. For each experiment, unless otherwise noted, results are reported as the mean ± SEM; sample sizes (both the number of neurons and the number of animals), statistical tests used, and *P* values are given either in the corresponding *Results* section or in the figure legends. For normally distributed data, a *t* test was used for pairwise comparisons, and a one-way ANOVA followed by Tukey's post hoc correction was used for multiple comparisons ($n > 2$ groups). For non-normally distributed data, a Wilcoxon sign rank (unpaired data) test or a Wilcoxon rank-sum (paired data) test was performed; a Wilcoxon rank-sum test with a Bonferroni post hoc correction was used for paired data with multiple comparisons, and a Kruskal–Wallis test followed by Tukey's post hoc correction was used for multiple comparisons with unpaired data. For statistical tests that involved a Bonferroni correction for multiple comparisons, *P* values above 1 were replaced with 1. For distribution comparisons, a two-sample Kolmogorov–Smirnov test was used. Results were considered significant if $P < 0.05$. Significance symbols used in figures are defined as such: $*P < 0.05$; $**P < 0.01$; $***P < 0.001$; and n.s., $P > 0.05$.

Data, Materials, and Software Availability. Datasets used in all figures are posted publicly on figshare (55). Code generated and used for the analysis in this manuscript is posted publicly on Github (56). Code for mEPSC extraction from raw data can be found in Cary and Turrigiano (57). All other data are included in the manuscript and/or SI Appendix.

ACKNOWLEDGMENTS. This research was supported by NIH Grant 1F31EY031602-01 (J.B.) and NIH RO1 EY025613 (G.G.T.). In vivo spike extraction and initial processing were performed using Brandeis University's High Performance Computing Cluster which is partially funded by DMRMRSEC 1420382. We thank Alejandro Torrado Pacheco for invaluable mentorship and his work on the in vivo recording and analysis pipeline, Daniel Leman for in vivo experiment support, Lauren Tereshko for the empty vector control virus, and SciDraw for the rat illustration.

1. Nelson Abbott, Synaptic plasticity: Taming the beast. *Nat. Neurosci.* **3**, 1178–1183 (2000).
2. G. Turrigiano, S. Nelson, Homeostatic plasticity in the developing nervous system. *Nat. Rev. Neurosci.* **5**, 97–107 (2004).
3. J. Espinosa, M. Stryker, Development and plasticity of the primary visual cortex. *Neuron* **75**, 230–249 (2012).
4. K. Hengen, A. Torrado Pacheco, J. McGregor, S. Van Hooser, G. Turrigiano, Neuronal firing rate homeostasis is inhibited by sleep and promoted by wake. *Cell* **165**, 180–191 (2016).
5. Z. Ma, G. G. Turrigiano, R. Wessel, K. B. Hengen, Critical Dynamics are a homeostatic set point of cortical networks *in vivo*. *Neuron* **104**, 655–664.e4 (2019).
6. Y. K. Wu, K. B. Hengen, G. G. Turrigiano, J. Gjorgjieva, Homeostatic mechanisms regulate distinct aspects of cortical circuit dynamics. *Proc. Natl. Acad. Sci. U.S.A.* **117**, 24514–24525 (2020).
7. K. Hengen, M. Lambo, S. Van Hooser, D. Katz, G. Turrigiano, Firing rate homeostasis in visual cortex of freely behaving rodents. *Neuron* **80**, 335–342 (2013).
8. A. Torrado Pacheco, J. Bottorff, Y. Gao, G. G. Turrigiano, Sleep promotes downward firing rate homeostasis. *Neuron* **109**, 530–544.e6 (2021).
9. Turrigiano Lambo, Synaptic and intrinsic homeostatic mechanisms cooperate to increase L2/3 pyramidal neuron excitability during a late phase of critical period plasticity. *J. Neurosci.* **33**, 8810–8819 (2013).
10. T. Keck *et al.*, Synaptic scaling and homeostatic plasticity in the mouse visual cortex in vivo. *Neuron* **80**, 327–334 (2013).
11. W. Wen, G. G. Turrigiano, Developmental regulation of homeostatic plasticity in mouse primary visual cortex. *J. Neurosci.* **41**, 9891–9905 (2021).
12. V. Tatavarty *et al.*, Autism-associated shank3 is essential for homeostatic compensation in rodent V1. *Neuron* **106**, 769–777 (2020).
13. M. Steriade, I. Timofeev, F. Grenier, Natural waking and sleep states: A view from inside neocortical neurons. *J. Neurophysiol.* **85**, 1969–1985 (2001).
14. B. Jones, From waking to sleeping: Neuronal and chemical substrates. *Trends Pharmacol. Sci.* **26**, 578–586 (2005).
15. S. Lee, Y. Dan, Neuromodulation of brain states. *Neuron* **76**, 209–222 (2012).
16. Y. Han *et al.*, Selective activation of cholinergic basal forebrain neurons induces immediate sleep–wake transitions. *Curr. Biol.* **24**, 693–698 (2014).
17. J. Zant *et al.*, Cholinergic neurons in the basal forebrain promote wakefulness by actions on neighboring non-cholinergic neurons: an opto-dialysis study. *J. Neurosci.* **36**, 2057–2067 (2016).
18. Singer Bear, Modulation of visual cortical plasticity by acetylcholine and noradrenaline. *Nature* **320**, 172–176 (1986).
19. M. Kaneko, D. Stellwagen, R. Malenka, M. Stryker, Tumor necrosis factor-alpha mediates one component of competitive, experience-dependent plasticity in developing visual cortex. *Neuron* **58**, 673–680 (2008).
20. L. Pinto *et al.*, Fast modulation of visual perception by basal forebrain cholinergic neurons. *Nat. Neurosci.* **16**, 1857–1863 (2014).
21. J. Kang, F. Huppe-Gourgues, E. Vaucher, Pharmacological mechanisms of cortical enhancement induced by the repetitive pairing of visual/cholinergic stimulation. *PLoS ONE* **10**, 1–18 (2015).
22. M. Lee, O. Hassani, A. Alonso, B. Jones, Cholinergic basal forebrain neurons burst with theta during waking and paradoxical sleep. *J. Neurosci.* **25**, 4365–4369 (2005).
23. M. Xu *et al.*, Basal forebrain circuit for sleep–wake control. *Nat. Neurosci.* **18**, 1641–1647 (2015).
24. J. Kim *et al.*, Selectivity of neuromodulatory projections from the basal forebrain and locus ceruleus to primary sensory cortices. *J. Neurosci.* **36**, 5314–5327 (2016).
25. G. Buzsaki *et al.*, Nucleus basalis and thalamic control of neocortical activity in the freely moving rat. *J. Neurosci.* **8**, 4007–4026 (1988).
26. L. Chen *et al.*, Basal forebrain cholinergic neurons primarily contribute to inhibition of EEG delta activity, rather than inducing behavioral wakefulness in mice. *Neuropschopharmacology* **41**, 2133–2146 (2016).
27. C. Blanco-Centurion, A. Shiromani, E. Winston, P. Shiromani, Effects of hypocretin-1 in 192-IgG-saporin-lesioned rats. *Eur. J. Neurosci.* **24**, 2084–2088 (2006).
28. S. Kaur, A. Junek, M. Black, K. Semba, Effects of ibotenate and 192IgG-Saporin lesions of the nucleus basalis magnocellularis/substantia innominate on spontaneous sleep and wake states and on recovery sleep after sleep deprivation in rats. *J. Neurosci.* **28**, 491–504 (2008).
29. P. Fuller, D. Sherman, N. Pedersen, C. Saper, J. Lu, Reassessment of the structural basis of the ascending arousal system. *J. Comp. Neurol.* **519**, 933–956 (2010).
30. A. Maffei, G. Turrigiano, Multiple modes of network homeostasis in visual cortical layer 2/3. *J. Neurosci.* **28**, 4377–4384 (2008).
31. N. Trojanowski, J. Bottorff, G. Turrigiano, Activity labeling in vivo using CaMPARI2 reveals intrinsic and synaptic differences between neurons with high and low firing rate set points. *Neuron* **109**, 663–676 (2021).
32. A. Levey, C. Kitt, W. Simonds, D. Price, M. Brann, Identification and localization of muscarinic acetylcholine receptor proteins in brain with subtype-specific antibodies. *J. Neurosci.* **11**, 3218–3226 (1991).
33. M. Yamasaki, M. Matsui, M. Watanabe, Preferential localization of muscarinic M1 receptor on dendritic shaft and spine of cortical pyramidal cells and its anatomical evidence for volume transmission. *J. Neurosci.* **30**, 4408–4418 (2010).
34. M. Groleau, J. Kang, F. Huppe-Gourgues, E. Vaucher, Distribution and effects of the muscarinic receptor subtypes in the primary visual cortex. *Front. Synaptic Neurosci.* **7**, 10 (2015).
35. B. Chattopadhyaya *et al.*, Experience and activity-dependent maturation of perisomatic GABAergic innervation in primary visual cortex during a postnatal critical period. *J. Neurosci.* **24**, 9598–9611 (2004).
36. M. Nahmani, G. Turrigiano, Deprivation-induced strengthening of presynaptic and postsynaptic inhibitory transmission in layer 4 of visual cortex during the critical period. *J. Neurosci.* **34**, 2571–2582 (2014).
37. Stuart Gulledge, Cholinergic inhibition of neocortical pyramidal neurons. *J. Neurosci.* **25**, 10308–10320 (2005).
38. A. Gulledge, D. Bucci, S. Zhang, M. Matsui, H. Yeh, M1 receptors mediate cholinergic modulation of excitability in neocortical pyramidal neurons. *J. Neurosci.* **29**, 9888–9902 (2009).
39. Bruno Constantinople, Effects and mechanisms of wakefulness on local cortical networks. *Neuron* **69**, 1061–1068 (2011).
40. S. Maurer, C. Williams, The cholinergic system modulates memory and hippocampal plasticity via its interactions with non-neuronal cells. *Front. Immunol.* **8**, 1489 (2017).
41. A. Kirkwood, C. Rozas, J. Kirkwood, F. Perez, M. Bear, Modulation of long-term synaptic depression in visual cortex by acetylcholine and norepinephrine. *J. Neurosci.* **19**, 1599–1609 (1999).
42. D. Caruana, C. Warburton, Z. Bashir, Induction of activity-dependent LTD requires muscarinic receptor activation in medial prefrontal cortex. *J. Neurosci.* **31**, 18464–18478 (2011).
43. M. Picciotto, M. Higley, Y. Mineur, Acetylcholine as a neuromodulator: Cholinergic signaling shapes nervous system function and behavior. *Neuron* **76**, 116–129 (2012).
44. Dan Alitto, Cell-type-specific modulation of neocortical activity by basal forebrain input. *Front. Syst. Neurosci.* **9**, 79 (2013).
45. H. D. Diering *et al.*, Homer1a drives homeostatic scaling-down of excitatory sunapses during sleep. *Science* **355**, 511–515 (2017).
46. M. A. Gainey, J. W. Aman, D. E. Feldman, Rapid disinhibition by adjustment of PV intrinsic excitability during whisker map plasticity in mouse S1. *J. Neurosci.* **38**, 4746–4749 (2018).
47. M. A. Gainey, D. E. Feldman, Multiple shared mechanisms for homeostatic plasticity in rodent somatosensory and visual cortex. *Philos. Trans. R Soc. Lond. B, Biol. Sci.* **372**, 20160157 (2017).
48. K. Nataraj, N. Le Roux, M. Nahmani, S. Lefort, G. Turrigiano, Visual deprivation suppresses L5 pyramidal neuron excitability by preventing the induction of intrinsic plasticity. *Neuron* **68**, 750–762 (2010).
49. K. Nataraj, G. Turrigiano, Regional and temporal specificity of intrinsic plasticity mechanisms in rodent primary visual cortex. *J. Neurosci.* **31**, 17932–17940 (2011).
50. B. Bloem *et al.*, Topographic mapping between basal forebrain cholinergic neurons and the medial prefrontal cortex in mice. *J. Neurosci.* **34**, 16234–16246 (2014).
51. T. Kim *et al.*, Cortically projecting basal forebrain parvalbumin neurons regulate cortical gamma band oscillations. *Proc. Natl. Acad. Sci. U.S.A.* **112**, 3535–3540 (2015).
52. I. Witten *et al.*, Recombinase-driver rat lines: Tools, techniques, and optogenetic application to dopamine-mediated reinforcement. *Neuron* **72**, 721–733 (2011).
53. Watson Paxinos, *The Rat Brain in Stereotaxic Coordinates* (Academic Press, Inc., ed. 4, 1998).
54. A. Mathis *et al.*, DeepLabCut: Markerless pose estimation of user-defined body parts with deep learning. *Nat. Neurosci.* **21**, 1281–1289 (2018).
55. J. Bottorff, G. Turrigiano, Basal Forebrain Cholinergic Activity is Necessary for Upward Firing Rate Homeostasis in Rodent Visual Cortex. FigShare: https://figshare.com/projects/Basal_Forebrain_Cholinergic_Activity_is_Necessary_for_Upward_Firing_Rate_Homeostasis_in_Rodent_Visual_Cortex/187710. Deposited 4 December 2023.
56. J. Bottorff, G. Turrigiano, turrigianoCodeSpace/JB_PNAS_paper. Github: https://github.com/turrigianoCodeSpace/JB_PNAS_paper. Deposited 4 December 2023.
57. C. Turrigiano, Stability of neocortical synapses across sleep and wake states during the critical period in rats. *eLife* **10**, e66304 (2021).